Proceedings of the 3rd International Conference on Environmental Geoscience and Earth Ecology
DOI: 10.54254/2753-8818/94/2025.22226

A CRISPR-RCA Enhanced Ru-doped Nanophosphor for Cd^{2+} Detection in Seafood

Allison Wang

Shanghai American School, Shanghai, China
allisonwang03@gmail.com

Abstract: Seafood products play a vital role in human dietary. Developing highly sensitive and rapid-response detection strategies is crucial for ensuring the seafood safety and safeguarding public health. In this study, I developed a novel signal-amplified, in-situ, and highly sensitive fluorescence detection platform based on rolling circle amplification (RCA)-assisted CRISPR technology for the efficient detection of cadmium ions (Cd^{2+}) in raw shrimp seafood. $Ru(bpy)_3^{2+}$ doped SiO_2 (RuSi) nanoparticles are employed as fluorescent probes in conjunction with reporting probes. In the presence of Cd^{2+}, aptamers bind to Cd^{2+}, thereby releasing the primer probe. Stimulated by the primer, the PC3 probe interacts with Phi29 enzyme to induce highly efficient RCA, significantly increasing the number of PC3 fragments in the system. These generated fragments then associate with NTS probes, Cas12, and CrRNA to form CRISPR complexes capable of non-specific single-strand cleavage. These complexes cleave the complementary probe BP of RP in the system, preventing the formation of double-stranded structures between RuSi QDs-RP complexes and BP. Consequently, RuSi QDs form single-strand-graphene complexes with reduced graphene oxide on the substrate surface, generating fluorescence. Under optimized conditions, the sensor exhibits a good linear response to Cd^{2+} with a detection sensitivity of 1 nM. Furthermore, using this detection system, I designed an integrated fluorescence detector for sample injection, detection, and signal readout. The sensor, powered by an STM32 chip, recognizes fluorescence signals and monitors Cd^{2+} concentrations in real-time through an LCD display. This sensing device offers advantages such as instant concentration display, portability, and high sensitivity, holding promising prospects for application in the field of food safety detection.

Keywords: Fluorescence biosensing, seafood, CRISPR, RCA, Signal amplification.

1. Introduction

Seafood is a common source of sustenance in many regions of the world, serving as part of a healthy and nutritious diet. In 2023, seafood sales in China increased by 3.5% compared to 2022, reaching up to 71 million metric tons (MMT). This reflects a growing demand for seafood that are nutritious and safe for consumption. However, increasing heavy metal contaminants are found in the marine system, affecting food chains [1]. Excessive bioaccumulation of heavy metal content is compounded by biomagnification along the food chain, resulting in exceedingly high levels of metal content in higher trophic levels [2,3].

Growing up in China Taiwan, a small island surrounded by the sea, I have always been eating seafood such as the squids from Fujian. However, as I became more aware of environmental issues,

© 2025 The Authors. This is an open access article distributed under the terms of the Creative Commons Attribution License 4.0 (https://creativecommons.org/licenses/by/4.0/).

DOI: 10.54254/2753-8818/94/2025.22226

I learned about the different health risks associated with food safety. Dr. Jiang, a nephrologist and CEO of the seafood company from which my family regularly purchases, said that China Taiwan has one of the highest rates of kidney dialysis in the world due to the high levels of heavy metals released caused by industrial development in this region. Upon accumulating in seafood, the heavy metal contents can severely impact consumers. This is a global issue affecting not just China, but other seafood-dependent nations like Japan and the Philippines [4]. Ingesting seafood containing excessive heavy metals amount can lead to short term effects such as vomiting, diarrhea, heavy metal poisoning, and shock. Long term effects include an increased risk of neurological disorders, cancer, degenerative bone disease, kidney and liver damage, gastrointestinal disorders, lungs injuries, and circulatory system problems [5]. This issue demands critical attention as the State Council of the People's Republic of China's new policies put emphasis on food safety supervision technology and strict on-site detection of business operations. Through developing effective monitoring detectors, the levels of unwanted and harmful substances in food can be reduced, and consumer health can be remarkably improved. To achieve this, detection performances should be enhanced by upgrading portable, highly sensitive, and accurate aspects in detection.

The main methods currently used to measure heavy metal ions in seafood include mass spectrometry, atomic absorption spectroscopy [6], colorimetry, and fluorescence methods [7,8]. Mass spectrometry is accurate but time-consuming, requires complex preparation and operation processes, demands expensive equipment, and needs professional operators [9]. Colorimetry has a simple testing method with a straightforward procedure and relatively lower costs, but its results are inaccurate, prone to false positives and negatives, and can only provide semi-quantitative analysis, not precise quantification [10]. Fluorescence spectrometry, on the other hand, is a photoluminescence detection technology, that offers high sensitivity, rapid response, and quantitative analysis capabilities, and has been widely used in the detection of heavy metal ions in seafood. Haoyang He's group developed an "on-off-on" fluorescent nanosensing detector that has a wide detection range in foods[11]. However, the "on-off-on" fluorescent sensor can't achieve real-time and on-site detection, as well as photostability. Yizhong Shen's group built a smartphone based ratiometric fluorescent food sensor in food safety setting [12]. It is a portable sensor that can achieve onsite visual detection. Despite that, it requires complex sample preparation as well as has inconsistent image signal processing.

Although the current reports have achieved acceptable performances in food safety detection, there still remains room for enhancing fluorescence techniques since the targets heavy metal ions often exhibited low concentrations. To address this, signal amplification technologies such as CRISPR (Clustered Regularly Interspaced Short Palindromic Repeats) and RCA (rolling cyclic amplification), can be used to significantly enhance the signal of the target substance, amplifying the sensitivity of fluorescence detection.

CRISPR technology is a gene-editing technique that is capable of precisely modifying DNA sequences and regulating gene activity [13-15]. It has a high precision, simple operation, relatively low cost, and can be applied in disease treatment, genetic disease research, crop improvement, etc [16]. RCA technology, or Rolling Circle Amplification, is a DNA-based signal amplification technique that can replicate large amounts of DNA [17,18]. It is commonly used in molecular diagnostics, biomarker detection, and genetic testing due to its high efficiency, high specificity, as well of simple operation [19,20]. By combining CRISPR and RCA technologies for fluorescence detection, a highly sensitive detection of low-concentration heavy metal ions can be achieved. The high specificity of CRISPR can be used to identify specific heavy metal ion DNA sequences, while RCA can effectively amplify these sequences [21], significantly enhancing the signal and thus improving detection sensitivity. This complex is relatively rare in fluorescence detection, making it significant to research.

DOI: 10.54254/2753-8818/94/2025.22226

In this work, a novel biosensor was developed for the detection of heavy metal content Cd^{2+} in seafood products. CRISPR and RCA technologies were incorporated to develop a highly sensitive, selective, and accurate fluorescent detector. The system comprises of three parts — signal detection through aptamer, signal amplification through RCA reaction, and signal display through CRISPR-controlled nanoparticle fluorescence. Firstly, a primer-aptamer complex was formed, which binds to Cadmium ions and generates an aptamer-Cd^{2+} complex. The primer was released consequently, allowing the formation of a complex with the PC3 probes. In presence of Phi29 enzyme, the RCA reaction was initiated, forming a complex with large amounts of PC3 probe fragments. The PC3 fragments in the DNA complex can combine with the NTS probes, which forms the Cas12a/crRNA complex with the crRNA and cas12a enzyme. The Cas12a/crRNA complex possesses nonspecific single-stranded DNA (ssDNA) cleavage activity, leading to continuous cleavage of ssDNA in the reaction solution. Consequently, the BP probes in the solution will be completely cleaved. Under these circumstances, the subsequent RuSi QDs-RP probes added onto the substrates will be unable to form complementary DNA complexes with the BP single strand. As a result, the RuSi QDs-RP will combine with the rGO on the electrode by the electrostatic absorption, leading to the fluorescence emission. This type of fluorescent signal changes is directly proportional to the Cd^{2+} concentrations. Under optimal conditions, this fluorescent-based sensor paired with the CRISPR-RCA amplification technology can show highly-sensitive detection performances of Cd^{2+} in seafood. In addition, by integrating the chip technology with sample addition, detection, and signal readout into a unified system, this portable food safety detection device enables in situ, real-time, and highly sensitive detection of heavy metal ions, offering broad application prospects in the field of food safety.

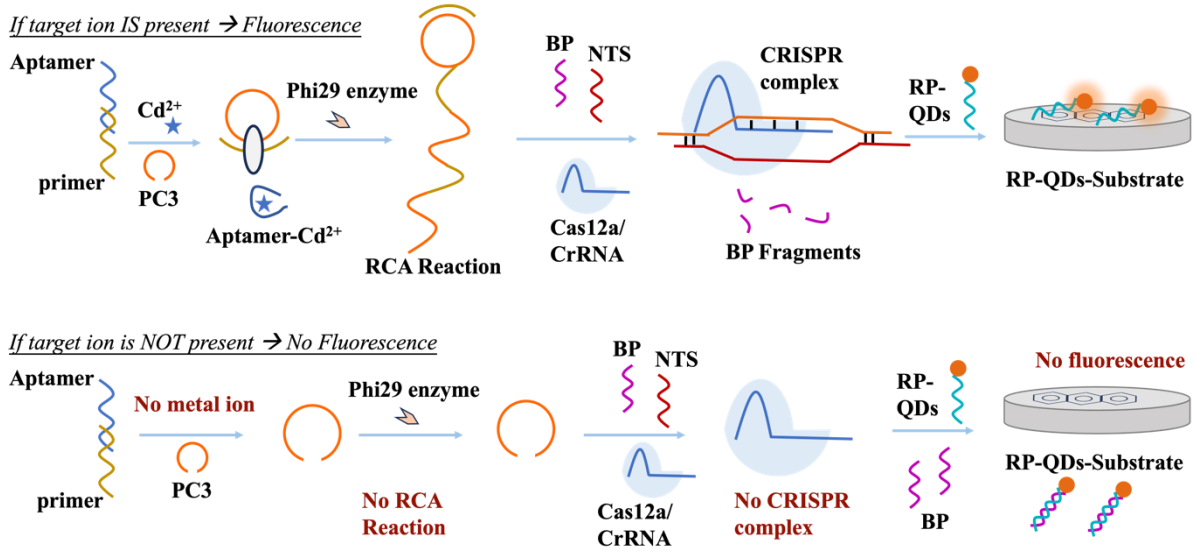


Figure 1: The scheme illustration of the CRISPR and RCA based fluorescence apparatus for highly sensitive detection of Cd^{2+}

2. Experiment Section

2.1. Reagents

1× PBS, $Ru(bpy_3)^{2+}$, Triton 100, NH_3-H_2O, TEOS, T4-DNA ligase, T4-DNA ligase buffer, phi29 DNA polymerase, phi29 DNA buffer, dNTPs, cas12a protein, cas12 reaction buffer, APTES, EDC/NHS, DEPC water (RNA enzyme free water), DNA and RNA sequences were purchased from Sangon biotechnology, Shanghai, China and were listed in Table 1.

DOI: 10.54254/2753-8818/94/2025.22226

Table 1: The DNA and RNA sequences used in this experiment

DNA name	DNA sequences
Primer	ATA CTC CCC CCA GGT CTT AGT CGC AA
Cd2+ Aptamer	TAG CTT ATC AGA CTG ATG TTG A
PC3	ACC TGG GGG AGT TCA ACA TAC TTT GAT CAC GGA TTC ACT TGA GCG ACA ATT TGC GAC TAA G
NTS	TTCA ACA TAC TTTG ATC ACG GAT TC ACT TGA GC GAC AAT
CrRNA	AA UUU CUA CUG UUG UAG AU AUC ACG GAU UC ACU UGA GCG
RP	AAA AAT AAC AAG AAC AAA-QDs
BP	TTT GTT CTT GTT ATT TTT

2.2. Apparatus

Scanning electron microscopy (SEM), element distribution spectroscopy (EDS) and transmission electron microscopy (TEM) was used for collecting the morphology images of the nanomaterials. X-ray diffraction spectrum (XRD) was used for characterizing the crystal lattice of the nanoparticles. XPS was employed for detecting the components of the nanoparticles. CHI660E was used to applied the voltage for electrochemical reduction. Oscillator was used for mixing the solution. Ultrasonic cleaner was applied to disperse the nanoparticles. Centrifuge, oven, hotting plate and magnetic stirrer were employed for the synthesis for the nanoparticles. Lab Ultrapure Water Systems was used to provide the ultrapure water throughout the experiments. Ultraviolet Analyzer was used for collecting the fluorescence visual images. PCR Machine was used for carrying out the DNA reactions.

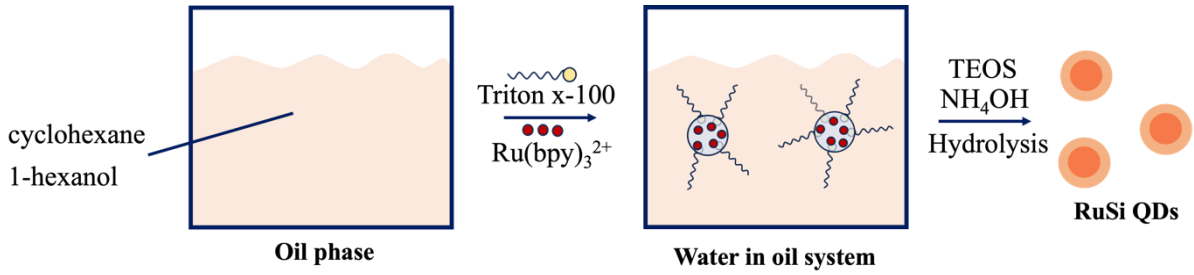


Figure 2: The scheme illustration for the synthesis of RuSi QDs using water-in-oil microemulsions

2.3. Preparation of the Ru doped silica nanoparticles (RuSi NPs)

Water-in-oil microemulsions, or reverse micelles method is used to synthesize RuSi nanoparticles. 7.5 mL cyclohexane and 1.8mL 1-hexanol were added in a flask, creating an oil-based solution. 1.77 mL of the surfactant triton x-100, and 340 uL $Ru(bpy)_3^{2+}$ (40 mM) were mixed and stirred, generating a water-in-oil microemulsion. Then, TEOS and NH_4OH were added to undergo hydrolysis reaction, and the mixture was allowed to react for 24 h in the dark. Next, acetone was added to break the emulsion, following by centrifuging and washing the nanoparticles with ethanol and water. The obtained orange-colored RuSi QDs were stored in 4°C for later use.

2.4. The preparation of real shrimp samples

Slightly smash the raw shrimp sample and immerse it into 1X Phosphate Buffered Saline (PBS) solution for 3 hours. Take out the shrimp, centrifuge the resulting PBS sample solution at 4000 r/min for 15 minutes. Remove the solid impurities from the sample solution and take the supernatant as a blank sample for testing. Standard addition method is used to control the cadmium concentration.

DOI: 10.54254/2753-8818/94/2025.22226

Take 2 mL of the blank actual sample and add desired concentrations and volume of Cd^{2+} standard solution. Shrimp samples with cadmium concentrations of 10 nM, 50 nM, and 100 nM were formed.

2.5. The preparation of the fluorescence reaction probe

20 μL of 1.0 μM aptamer and 20 μL of 1.0 μM primer were added in an Eppendorf tube, and put in a Polymerase Chain Reaction (PCR) machine at 37 degrees Celsius (℃) for 1 hour. To create a PC3-Primer DNA complex, 10 μL of 10 U T4 enzyme and 20 μL of 0.5 μM PC3 were added in the aptamer-primer solution, and put in a PCR machine at 30 ℃. After incubated for 40 minutes, 6 μL of 10 U Phi 29 enzyme and 20 μL of 10 μM Cd^{2+} were introduced in the PC3-Primer DNA complex, and put in a PCR machine at 30 degrees Celsius for 40 minutes and 65℃ for 10 minutes to terminate the reaction. 20 μL of 5 μM BP, 20 μl of 1 μM NTS, and 22 μl of 100 nM Cas12 CrRNA were added to the Phi29-Cd mixture to prepare for CRISPR amplification. The mixture was placed in a PCR machine at 37 ℃ for 1 hour. 50 μL 2 mg/mL of QDs were added in the mixture and put in a PCR machine at 37 ℃ for 30 minutes.

2.6. Electrode modification

To allow better binding of the RuSi quantum dots with the glass electrode, the electrode was modified with reduced graphene oxide (rGO). Then, it was dried in the oven at 45 ℃ for 1 hour to ensure the complete attachment of graphene oxide onto the surface of the glass electrode.

2.7. Fluorescence detection

The DNA product obtained through CRISPR and RCA amplification was added onto the surface of the glass electrode modified with rGO and incubated at 37 ℃ for 1 hour. The RuSi QDs-RP probe was added and incubated overnight at room temperature. The modified electrode was washed with PBS buffer, and then analyzed using a Fluorescence spectrometer and a UV spectrophotometer. Image-Pro software was further used to analyze the integrated optical density of the fluorescence signals.

2.8. The assembly of the integrated fluorescence apparatus

The Fluorescent detector consists of sample introduction system, detection system, and signal readout system. Sample introduction system includes a glass electrode modified with reduced graphene oxide and a detection kit. The detection kit includes aptamer detection, Rolling Circle Amplification, CRISPR system. The RuSi-RP quantum dots is mixed and incubated with the system, forming the surface of the electrode that will be tested. In detection system, the test buttons are controlled by the STM32 system interface. Upon initiation, the generated fluorescence is transmitted through the optical pathway to the light intensity sensor of the STM32 chip, resulting in a readout on the LCD display.

3. Result and Discussion

3.1. Morphology and optical characterization of the RuSi fluorescence probes

Figure 3 shows the morphology of the RuSi nanoparticles obtained through scanning electron microscope. RuSi nanoparticles exhibit uniform particle sizes, approximately 40 nm. This image demonstrates a uniform particle size with minimal aggregation, ensuring a stable fluorescence signal output.

DOI: 10.54254/2753-8818/94/2025.22226

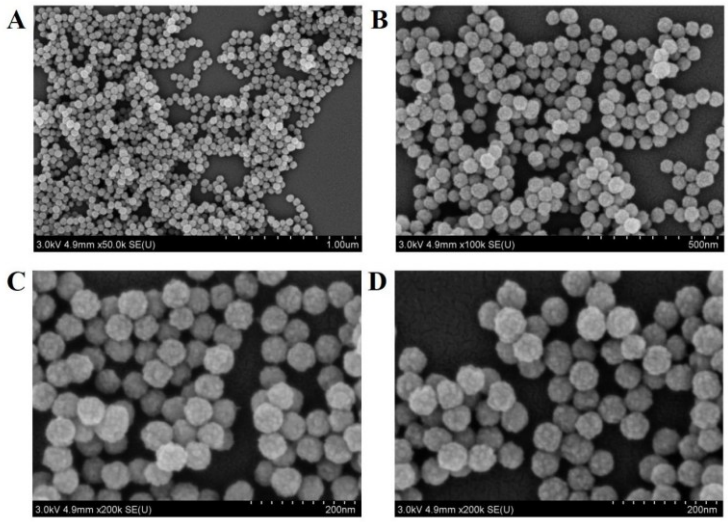


Figure 3: Scanning Electron Microscopy (SEM) images of RuSi Quantum Dots under different magnifications (A) 1.0 um; (B) 500 nm; (C) 200nm; (D) 200nm.

The 200 nm scale image reveals a rough surface texture, increasing the surface area and loading capacity of the quantum dots. This allows for the attachment of more $Ru(bpy)_3^{2+}$ molecules and facilitates better single-stranded DNA attachment, which enhanced the fluorescence signal.

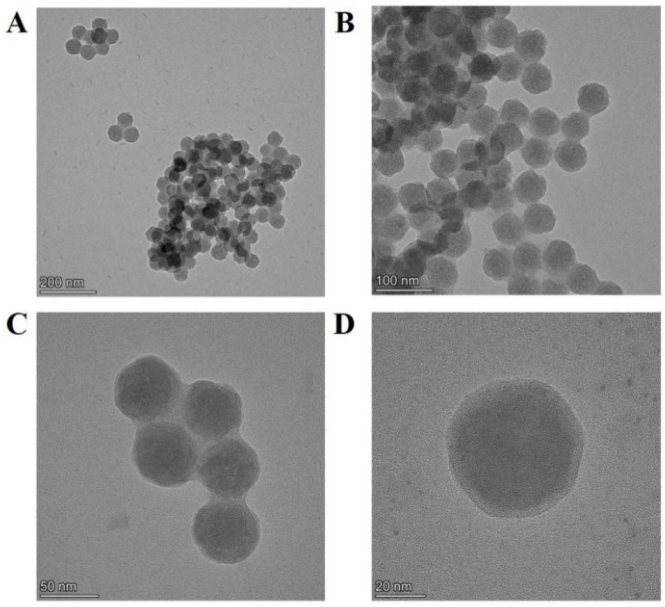


Figure 4: The TEM observation of the RuSi QDs at different scale. (A) 200nm; (B) 100nm; (C) 50 nm; (D) 20nm;

The TEM observations of the RuSi QDs were displayed in Figure 4. It is seen that the RuSi QDs exhibited superior homogeneity at different scale with an average diameter of 40 nm, which corresponded well with the SEM images. At the scale of the 50 nm and 20 nm, it is observed that the RuSi QDs possessed core-shell structure. The out layer of the core-shell structure showed low contrast while the inner layer disappeared high contrast, which exhibited high consistency with the previous literature. In order to further study the microstructure, the TEM-EDS mapping of RuSi NPs was conducted.

DOI: 10.54254/2753-8818/94/2025.22226

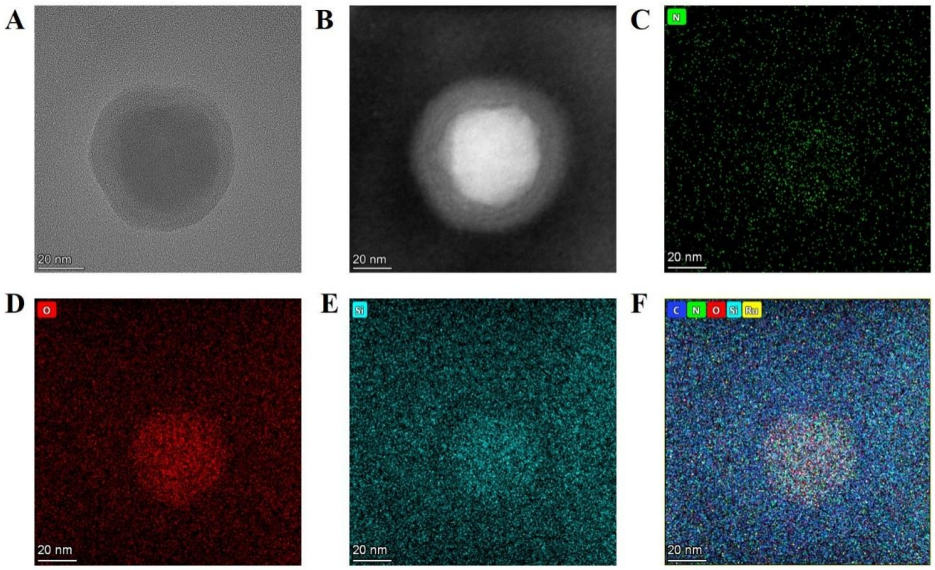


Figure 5: The Energy Dispersive Spectroscopy (EDS) mapping of the RuSi QDs. (A) The TEM image of the RuSi QDs in Bright-Field Mode (B) The TEM image of RuSi in Dark-Field Mode (C) The N element mapping of RuSi QDs. (D) The O element mapping of the RuSi QDs. (E) The Si element mapping of the RuSi QDs. (F) The mixed mapping contains C, N, O, Si, and Ru elements of RuSi QDs.

As shown in Figure 5, at different transmission modes, the RuSi QDs both exhibited obvious core-shell structures (Figure 5A and 5B). The subsequent element mapping suggested that the C, N, O, and Si elements of RuSi QDs distributed a good overlap and showed acceptable consistency with the TEM images, which proved the existence of the C, N, O, and Si elements in the structure of RuSi QDs.

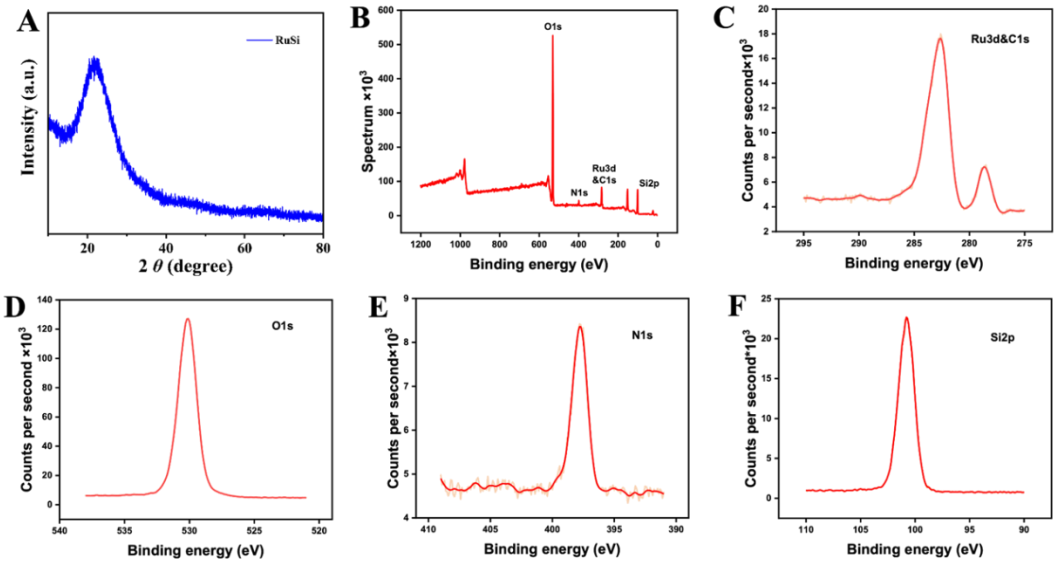


Figure 6: The XRD and XPS spectrum of the RuSi QDs. (A) the XRD spectrum of the RuSi QDs. (B) the wide measurements of the XPS spectrum of the RuSi QDs. (C-F) the magnified spectrum of the N, Si, Ru, C and O measurement of the XPS spectrum of the RuSi QDs.

DOI: 10.54254/2753-8818/94/2025.22226

The XRD and XPS spectral characterization data of RuSi QDs are presented in Figure 6. Figure 6A displays the XRD diffraction spectrum of the RuSi QDs, revealing a broad absorption peak at 24°, which is attributed to the XRD diffraction peak of fine SiO_2 nanoparticles. The appearance of this broad peak in the XRD spectrum indicates the presence of fine SiO_2 particles within the structure of the RuSi QDs, particularly when a large number of these particles aggregate. Figure 6B shows the wide-spectrum XPS scan of the RuSi QDs, indicating the inclusion of elements such as Si, O, N, Ru, and C in the structure. Figure 6C presents a locally magnified XPS energy spectrum curve for the N element, exhibiting an energy peak at 398 eV, corresponding to the 1s orbital transition of N. Figures 6D and 6F depict locally magnified XPS energy spectrum curves for the Si and O elements, respectively, with broad XPS absorption peaks at 101 eV and 530 eV, representing the 2p orbital transition of Si and the 1s orbital transition of O. Figure 4E displays a mixed XPS energy spectrum curve for the Ru and C elements. Due to the similar transition energies of the 3d orbital of Ru and the 1s orbital of C, the spectral peaks of these two elements overlap in the XPS spectrum. The XRD and XPS analyses confirm the successful preparation of RuSi QDs, which consist of elements such as Si, O, N, and Ru, with fine SiO_2 particles encapsulating $Ru(bpy)_3^{2+}$ molecules.

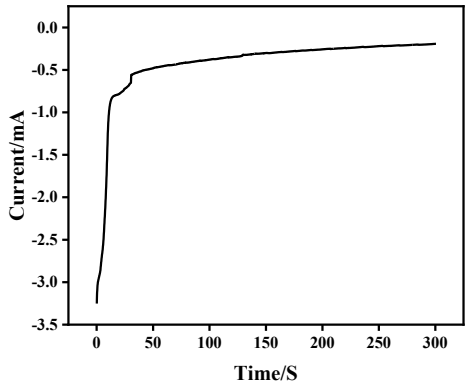


Figure 7: The electrochemical reduction of the Graphene Oxide at -0.5 V for 300 s.

3.2. The detection principle of the developed RCA assisted CRISPR assay

In order to achieve the rGO structure at the glass carbon substrate, the GO modified glass carbon electrode was soaked in the 1X PBS solution. In the process of electrochemical reduction at the potential of -0.5V, the current-potential curve was obtained (Figure 7). It is clear that the electrochemical current decreased rapidly, indicating that the electrochemical reduction process was extremely fast and a large amount of GO was reduced to rGO in a short time. When the time approached 50 s, the electrochemical current gradually tended to stable, which was ascribed to the decreased amount of GO at the electrode surface and the hindrance of the electrochemical reduction by the generated GO structure.

Optimization and adjustment of the concentration of cadmium ions show that the strongest fluorescent activity occurs when a 25 4nm UV ray is emitted on a 10 μM concentration of cadmium ion through the ssDNA-rGO complement. Fluorescent images in 8b and 8c are acquired via a camera. Characteristics of a uniform fluorescence intensity, orange color, and circular shape are shown. Analysis of the fluorescent intensity through imagepro demonstrated that RuSi QD Fuorescence exhibits an IOD of 21.4k at 10μM cadmium ion concentration. Figure 8B depicts the stability of fluorescence in 5 parallel experiments under this concentration. The 5 experiments graphed in Figure 8B display little difference in the fluorescence intensity, proving it to be really stable to test real-life samples.

DOI: 10.54254/2753-8818/94/2025.22226

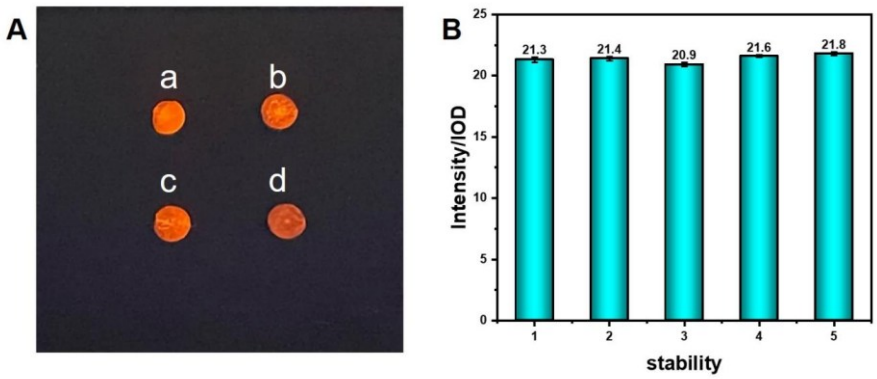


Figure 8: The fluorescence characterizations and stability of the RuSi QDs. (A) the fluorescence images of the RuSi QDs collected by the camera with different concentrations of Cd^{2+} (a and d, 1 μM; b and c, 10 μM). (B) the IOD intensity of the RuSi QDs after conducting the experiments at a concentration of 10 μM for 5 times.

3.3. Analysis performance of the developed biosensor

A highly sensitive ion fluorescence sensor is constructed based on the optimal signaling results of DNA via CRISPR and RCA technology. A directly proportional linear relation between Cd^{2+} and RuSi QDs is shown in figure 9A. As the concentration of Cd^{2+} increases, the fluorescent intensity of RuSi QDs also increases. The linear equation is y=1.24x+27.46, the linear regression coefficient is 0.997, and the detection limit of the sensor is 1nM. A selectivity analysis is also conducted on the fluorescence sensor, using a blank, Ca^{2+}, Mg^{2+}, and three mixed ions as interference factors for fluorescence intensity testing. As shown in Figure 8B, under the presence of Ca^{2+} and Mg^{2+}, there was not much difference in the fluorescent signals and blank signals, indicating that the aptamer does not respond to Ca^{2+} and Mg^{2+}. On the other hand, under the presence of Cd^{2+}, the fluorescent signal increased substantially, signifying that the sensor exhibits good selectivity towards different metal ions.

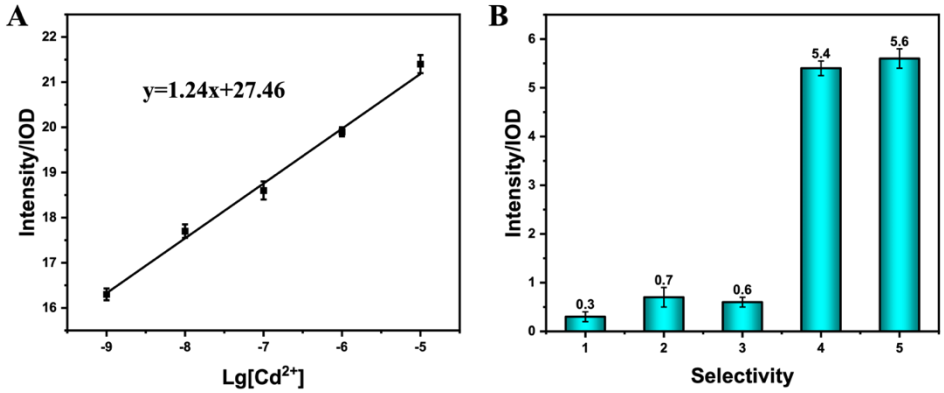


Figure 9: The linear relationship and selectivity of the developed biosensor. (A) the fluorescence intensity curves towards the logarithm of Cd^{2+} concentration. The concentration of Cd^{2+} was ranged from 10^{-9} to 10^{-5} M. (B) the fluorescence intensity changes compared with blank solution towards different disturb metal ions. (1: blank, 2: Ca^{2+}, 3: Mg^{2+}, 4: Cd^{2+} 5: the mixture of the Ca^{2+}, Mg^{2+} and Cd^{2+}).

DOI: 10.54254/2753-8818/94/2025.22226

Table 2: The recovery tests for the Cd^{2+} detection measurements in shrimp samples

Sample Number	Added (nM)	Intensity (IOD)	Found (nM)	R.S.D. (%)	Recovery (%)
1	10	17.53	9.72	4.57	97.2
2	50	18.39	48.76	3.71	97.5
3	100	18.79	101.33	2.98	101.3

3.4. Real sample analysis

The experiment with real samples was conducted through standard addition and recovery test using a blank shrimp extract as the matrix. Three concentrations of 10 nM, 50 nM, and 100 nM were selected to test the recovery rates of the blank real samples. The results are presented in Table 2. As shown in the table, when the added concentration was 10 nM, 9.72 nM of Cd^{2+} was detected, yielding a recovery rate of 97.2%. Furthermore, at added concentrations of 50 nM and 100 nM, the recovery rates reached 97.5% and 101.3%, respectively, indicating that the sensing method exhibits high recovery rates for real samples. Additionally, the errors between multiple experiments conducted under routine conditions were small, with relative standard deviations (R.S.D.) all below 5%. These test results fully demonstrate that the sensing method performs well in detecting real shrimp samples and holds promising application prospects in the field of food safety.

3.5. The construction of the innovative fluorescence apparatus

The integrated fluorescence detection device constructed through experiment section is illustrated in Figure 10. The device comprises three main components: sample introduction, testing, and signal readout. On the front of the device, there is an LCD display screen controlled by an STM32 development board. A sliding mobile sample tray is located on the right side of the device. When sample introduction is required, the internal sample tray can be opened using an external handle to place the sample, which is loaded on an ITO glass slide, inside. After placing the sample, a small internal UV light source within the instrument generates excitation UV light that irradiates the surface of the actual sample, producing fluorescence. As the intensity of the fluorescence signal is positively correlated with the concentration of Cd^{2+} in the sample, when the Cd^{2+} concentration increases, the fluorescence signal intensifies. The enhanced fluorescence signal can be recognized by the photosensitive element of the STM32 sensor within the instrument, allowing the readout to be displayed on the LCD screen. By establishing the correspondence between the readout changes and the concentration, we can construct a linear relationship between the fluorescence signal and the Cd^{2+} concentration within the STM32 development board, thereby achieving real-time, portable, and precise detection of Cd^{2+} concentration in food.

DOI: 10.54254/2753-8818/94/2025.22226

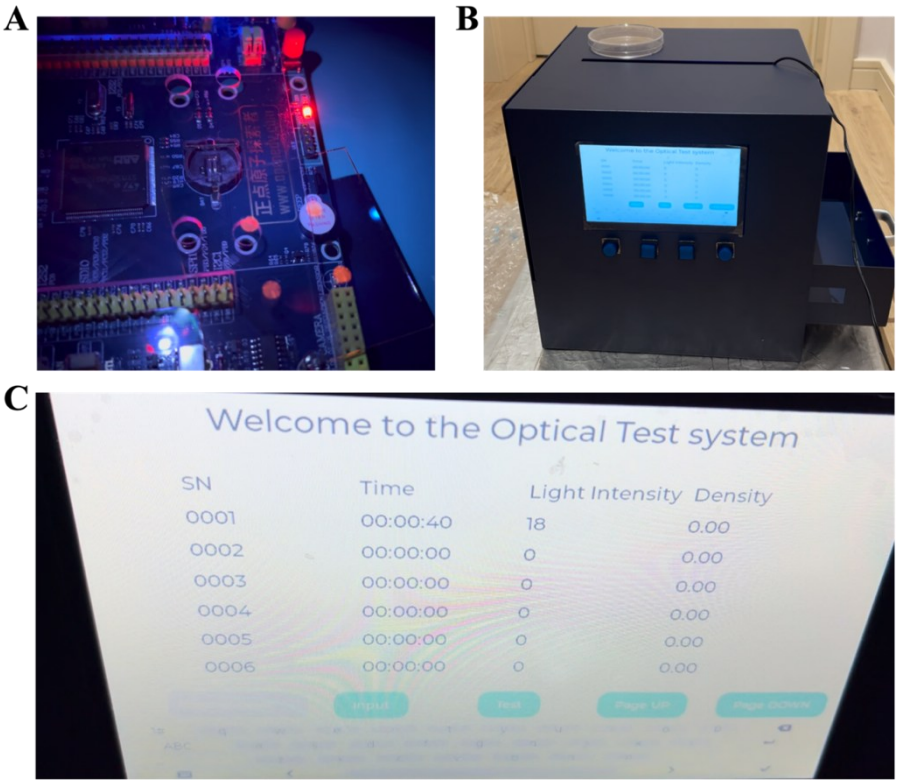


Figure 10: Photograph of fluorescence detection prototype. (A) STM32 Chip Board with glassy electrode piece. (B) Front view of Prototype with sample addition drawer. (C) LCD touch screen with light intensity display.

4. Conclusion

In this work, a heavy metal detector is created using CRISPR and RCA techniques in combination with fluorescence assay for highly sensitive detection of cadmium ions levels in seafood. The sensor exhibited good sensitivity as well as excellent selectivity, with a detection limit as low as 1 nM. The CRISPR-RCA amplification strategy can significantly enhance the detection performance of fluorescence-based detection systems, especially when targeting low-concentration objects. The detection system is portable and low-priced, making it suitable for food safety monitoring.

References

[1] *Zaynab, M., Al-Yahyai, R., Ameen, A., Sharif, Y., Ali, L., Fatima, M., . . . Li, S. (2022). Health and environmental effects of heavy metals. Journal of King Saud University-Science, 34(1), 101653.*

[2] *Yang, R., Feng, M., Liu, Z., & Liu, G. (2023). Trophic transfer and biomagnification of four heavy metals in freshwater food web: a case study of Zhangze Lake. Chemistry and Ecology, 39(9), 909-926.*

[3] *Hao, Z., Chen, L., Wang, C., Zou, X., Zheng, F., Feng, W., . . . Peng, L. (2019). Heavy metal distribution and bioaccumulation ability in marine organisms from coastal regions of Hainan and Zhoushan, China. Chemosphere, 226, 340-350.*

[4] *Cabuga, C., Rey, Y., & Jumawan, J. C. (2020). Levels of heavy metals in fish and sediments from different salinity gradients of lower Agusan River to Butuan Bay, Caraga, Philippines. EnvironmentAsia, 13, 88-100.*

[5] *Engwa, G. A., Ferdinand, P. U., Nwalo, F. N., & Unachukwu, M. N. (2019). Mechanism and health effects of heavy metal toxicity in humans. Poisoning in the modern world-new tricks for an old dog, 10, 70-90.*

[6] *Luo, Q., Gao, X., Hu, Y., Lin, K., Wang, X., & Cheng, H. (2019). Determination of methylmercury in rice using microwave-assisted extraction coupled with thermal decomposition amalgamation atomic absorption spectrometry (MAE-TDA-AAS). Analytical Methods, 11(10), 1361-1370.*

DOI: 10.54254/2753-8818/94/2025.22226

[7] Thakur, A., & Kumar, A. (2023). Recent trends in nanostructured carbon-based electrochemical sensors for the detection and remediation of persistent toxic substances in real-time analysis. Materials Research Express, 10(3), 034001.

[8] Mustatea, G., & Ungureanu, E. L. (2024). Assessing the presence and health risks of potentially toxic metals in food: a comprehensive overview.

[9] Lv, Y., Zhao, J., Xue, H., & Ma, Q. (2024). Ambient ionization mass spectrometry for food analysis: Recent progress and applications. TrAC Trends in Analytical Chemistry, 117814.

[10] Kim, E., Hahn, J., You, Y., & Choi, Y. J. (2024). Design and optimization of a colorimetric biosensor using functionalized gold nanoparticles and bi-functional linker for agriculture and food industry. Microchemical Journal, 111600.

[11] He, H., Sun, D.-W., Wu, Z., Pu, H., & Wei, Q. (2022). On-off-on fluorescent nanosensing: Materials, detection strategies and recent food applications. Trends in Food Science & Technology, 119, 243-256.

[12] Shen, Y., Wei, Y., Zhu, C., Cao, J., & Han, D.-M. (2022). Ratiometric fluorescent signals-driven smartphone-based portable sensors for onsite visual detection of food contaminants. Coordination Chemistry Reviews, 458, 214442.

[13] Xu, Y., Ma, J., Dai, C., Mao, Z., & Zhou, Y. (2024). CRISPR/Cas12a-drived electrochemiluminescence and fluorescence dual-mode magnetic biosensor for sensitive detection of Pseudomonas aeruginosa based on iridium (III) complex as luminophore. Biosensors and Bioelectronics, 116678.

[14] Wei, J., Zhang, J., Wang, W., Zhou, H., Ma, H., Gong, Y., . . . Liao, X. (2024). Precision miRNA profiling: Electrochemiluminescence powered by CRISPR-Cas13a and hybridization chain reaction. Analytica Chimica Acta, 1307, 342641.

[15] Zhu, Y. (2022). Advances in CRISPR/Cas9. BioMed research international, 2022(1), 9978571.

[16] Hosseini, S. A., Jouneghani, A. S., Ghatrehsamani, M., Yaghoobi, H., Elahian, F., & Mirzaei, S. A. (2022). CRISPR/Cas9 as precision and high-throughput genetic engineering tools in gastrointestinal cancer research and therapy. International Journal of Biological Macromolecules, 223, 732-754.

[17] Zhang, L., Jin, H., Zhang, Z., Bai, T., Wei, M., He, B., . . . Suo, Z. (2024). Triple-helix molecular-switch-actuated rolling circle amplification and catalytic hairpin assembly multistage signal amplified fluorescent aptasensor for detection of aflatoxin B1. Analytica Chimica Acta, 1323, 343072.

[18] Sun, M., Zhang, Y., Liu, C., Wang, Y., Wang, W., Wang, Z., . . . Wu, J. (2024). Allosteric probe-initiated double rolling circle amplification in tandem for sensitive whole-cell detection of E. coli O157: H7. Sensors and Actuators B: Chemical, 418, 136279.

[19] Garafutdinov, R., Sakhabutdinova, A., Gilvanov, A., & Chemeris, A. (2021). Rolling circle amplification as a universal method for the analysis of a wide range of biological targets. Russian Journal of Bioorganic Chemistry, 47, 1172-1189.

[20] Gu, L., Yan, W., Liu, L., Wang, S., Zhang, X., & Lyu, M. (2018). Research progress on rolling circle amplification (RCA)-based biomedical sensing. Pharmaceuticals, 11(2), 35.

[21] Hong, L.-R., Li, W., Lu, M.-Y., Xu, H., Liu, W., Zhu, Y., & Zhuo, Y. (2023). Simplified rolling circle amplification driven in situ generation of electrochemiluminescent silver nanoclusters for APE1 activity monitoring. Sensors and Actuators B: Chemical, 397, 134699.